OptiJ: Open-source optical projection tomography of large organ samples

Pedro P. Vallejo Ramirez[1], Joseph Zammit[2], Oliver Vanderpoorten[1,2], Fergus Riche[2], François-Xavier Blé[3], Xiao-Hong Zhou[4], Bogdan Spiridon[2], Christopher Valentine[2], Simeon P. Spasov[2], Pelumi W. Oluwasanya[2], Gemma Goodfellow[2], Marcus J. Fantham[1], Omid Siddiqui[2], Farah Alimagham[2], Miranda Robbins[2], Andrew Stretton[2], Dimitrios Simatos[2], Oliver Hadeler[1], Eric J. Rees[1], Florian Ströhl[1,6], Romain F. Laine[1,5], and Clemens F. Kaminski[1] ✉

[1]Laser Analytics Group, Department of Chemical Engineering and Biotechnology, University of Cambridge, Cambridge UK
[2]Sensor CDT 2015-2016 student cohort, University of Cambridge, Cambridge, UK
[3]Clinical Discovery Unit, Early Clinical Development, IMED Biotech Unit, AstraZeneca, Cambridge, UK
[4]Bioscience, Respiratory, Inflammation and Autoimmunity, IMED Biotech Unit, AstraZeneca, Gothenburg, Sweden
[5]Current address: Medical Research Council Laboratory for Molecular Cell Biology (LMCB), University College London, Gower Street, London, WC1E 6BT
[6]Current address: Department of Physics and Technology, UiT The Arctic University of Norway, NO-9037 Tromsø, Norway

The three-dimensional imaging of mesoscopic samples with Optical Projection Tomography (OPT) has become a powerful tool for biomedical phenotyping studies. OPT uses visible light to visualize the 3D morphology of large transparent samples. To enable a wider application of OPT, we present OptiJ, a low-cost, fully open-source OPT system capable of imaging large transparent specimens up to 13 mm tall and 8 mm deep with 50 µm resolution. OptiJ is based on off-the-shelf, easy-to-assemble optical components and an ImageJ plugin library for OPT data reconstruction. The software includes novel correction routines for uneven illumination and sample jitter in addition to CPU/GPU accelerated reconstruction for large datasets. We demonstrate the use of OptiJ to image and reconstruct cleared lung lobes from adult mice. We provide a detailed set of instructions to set up and use the OptiJ framework. Our hardware and software design are modular and easy to implement, allowing for further open microscopy developments for imaging large organ samples.

3D imaging | OPT | projection tomography | lungs | open-source | low-cost | large organs | ImageJ | Fiji

Correspondence: ***cfk23@cam.ac.uk***

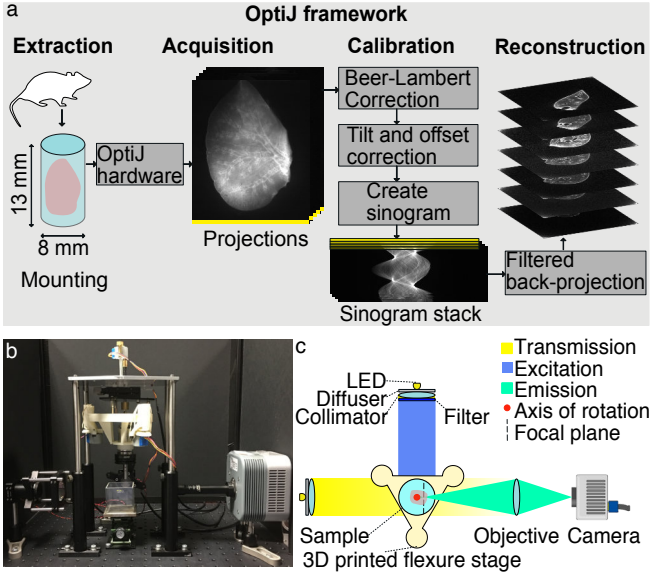

Fig. 1. Schematic representation of the OptiJ Framework. a) OptiJ workflow including sample mounting, acquisition of projections, correction, and reconstruction steps. **b)** Picture of the OptiJ set-up. **c)** Top-view illustration of the OptiJ hardware.

Introduction. The three-dimensional imaging of anatomical and functional features in mesoscopic biological samples (millimeter-scale dimensions) e.g. in model organisms, organs, or even plants, provides valuable data for biomedical research. Standard 3D imaging techniques such as micro-MRI (1–4) and micro-CT (5–9) are used in biomedical imaging to visualize morphology in large tissues and organs at micrometer-level resolution. However, these techniques are expensive and cannot take advantage of molecule-specific labeling strategies that are available to fluorescence microscopy. Confocal (10) or light sheet fluorescence microscopy (11–13) can be used to generate volumetric data with optical sectioning at sub-cellular resolution, although the usable specimen sizes are typically confined to sub-millimeter scales and commercial microscopy systems can be expensive. Optical Projection Tomography (OPT)(14) is a 3D imaging technique for transparent mesoscopic samples which allows visualizing micrometer-scale features. OPT is based on computerized tomography techniques (15) in which 2D images, called projections, are acquired with different sample orientations and then used to obtain a 3D image of the sample using a reconstruction algorithm, such as filtered-back projection (FBP). Sample clearing is often necessary to allow light propagation and imaging through the thickness of the sample. OPT can operate using either absorption/scattering of the sample (transmission OPT, tOPT) or fluorescence (emission OPT, eOPT) to generate image contrast. The use of OPT has been reported widely, and applications include the visualization of the 3D anatomy of mouse embryos (16–27), zebrafish (21, 24, 28–34), drosophila (35–38), plants (39, 40), *C.elegans* (41), animal organs (22, 27, 42–44) and other mesoscopic samples (45–47). Although major improvements in resolution (48, 49), acquisition time (31), field of view (FOV) (21, 40) and compatibility with other imaging techniques (22, 28, 50) have been made, most OPT applications require advanced technical expertise, expensive equipment, and bespoke software for reconstruction.

To enable a more general uptake of this technique, we present OptiJ (Fig. 1a-b), a low-cost, integrated, open-source implementation of OPT specifically designed to enable the

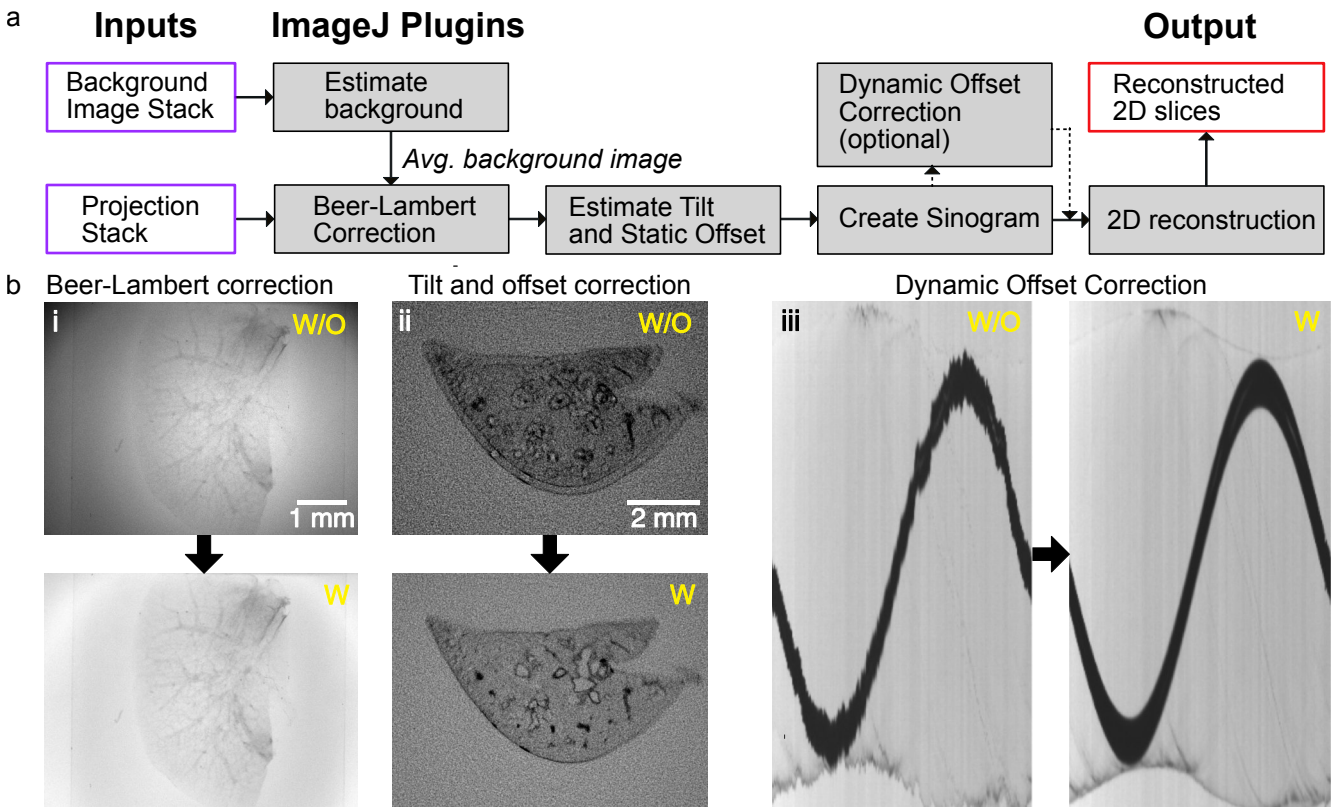

Fig. 2. OptiJ plugin library workflow for the correction of common OPT artifacts. a) Typical workflow for the use of the OptiJ plugins. **b)** Correction of common OPT artifacts using OptiJ plugins. The top row represents images without correction applied (w/o). The bottom row shows images after correction (w). (i) Uneven illumination in raw tOPT projections resulting from the optics used to collimate the light source, and absorption and scattering of the sample (ii) shadow artifact originating from a misalignment of the sample center of rotation. (iii) jittered sinogram of a marker bead rotated by a low-cost stepper motor.

3D imaging of large organ samples in both fluorescence and transmission modes. Our framework includes a complete set of open-source ImageJ/Fiji (51) plugins to reconstruct OPT data from specimens up to 13 mm tall and 8 mm deep (13x8x8 mm^3). A number of algorithms were developed to improve image quality. We include a thorough description of how to build and operate the hardware and how to use the software. Other open-source OPT implementations have been demonstrated for smaller volumes than what is necessary for large murine organs (24, 52), or for large volumes using commercial reconstruction software (21). Here, we demonstrate the capabilities of OptiJ by imaging full-sized adult mouse lungs that have been cleared and immunostained. Their study is relevant in the context of chronic obstructive pulmonary diseases (COPDs), which are characterized by heterogeneously distributed emphysema (alveolar cell death) and bronchoconstriction (narrowing of airways). OptiJ allowed us to explore the morphology of the airway tree and visualize in 3D the tertiary airways, bronchioles, and alveolar sacs in complete murine lungs. We share our results using FPBioimage (53), an open-source online visualization tool, so that readers can view and explore the reconstructed OPT data interactively in any standard web browser.

Results

OptiJ hardware. The OPT principle relies on the rotation of a sample to acquire 2D projections at different angles. Assuming the thickness of the sample is less than the depth of field of the system, projections acquired over half a revolution are theoretically sufficient to recover an accurate 3D reconstruction of the sample structure. However, a full revolution typically leads to higher image quality (14, 31). When implementing our OptiJ system, we focused on the following considerations: (1) ensuring that the axis of rotation is parallel to the imaging plane of the camera, (2) aligning the sample to the field of view of the camera, and (3) robustly and repeatably performing the rotation of the sample and acquisition of the projections. The OptiJ hardware enables the mounting, alignment, and rotation of thick biological samples for the acquisition of 2D projections in both eOPT and tOPT modalities. Figure 1b-c shows the implemented set up, which includes a monolithic 3D-printed rotation and translation stage, a telecentric relay lens, a camera, two broadband LEDs, fluorescence excitation and emission filters, and collimating and diffusing optics. The main criteria guiding our component choice were ease of access, widespread availability, and low cost. The 3D-printed stage is adapted from the published Flexscope design (54) to accomplish the movement necessary for both linear alignment and rotation of the sample with low-cost stepper motors. The stage achieves sub-micron steps, with a maximal hysteresis of 58 µm over a 3 mm travel range (see Supplementary Information for details on the stage characterization). A low numerical aperture (NA) 0.5x telecentric lens was chosen to match the typical volume of adult mouse lungs. The low NA allows a depth of field of ~4 mm,

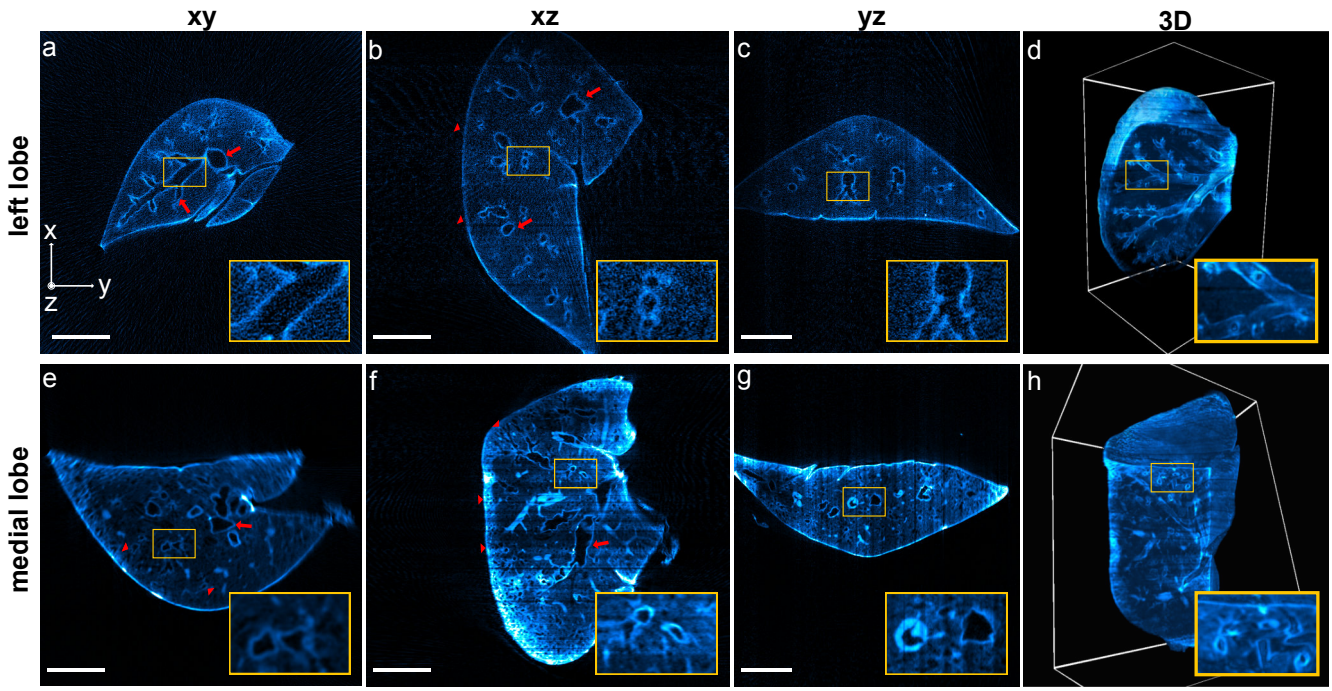

Fig. 3. OPT reconstructions of murine lungs. Reconstructions of a left lobe labelled with anti surfactant C – Alexa Fluor 488 (a-d) and a medial lobe labelled with anti TTF1 – Alexa Fluor 488 (e-h) from 512 eOPT projections, displayed in xy, xz, and yz orthogonal views (left three columns), as well as rendered in 3D (right-most column). **a-d)** The red arrows and the insets indicate the primary airways visualized in the orthogonal cross-sections. The 3D rendering in panel **d)** displays a clipping plane through the lung, highlighting secondary and tertiary bronchi in the inset. **e-h)** The red arrows indicate a set of main airways (secondary and tertiary bronchi) in the medial lobe, and red arrowheads indicate high-order airways inside or close to the parenchyma. Small airways close to the primary bronchi are highlighted in the insets on panels **e)** and **f)**. The 3D rendering in panel **h)** with a clipping plane on one of the lobe faces shows a thick meshwork of higher order airways (quaternary bronchi and bronchioles). Interactive 3D renderings are available in our online repository.

which upon sample rotation allows for a maximum field of view of 13x8x8 mm^3. The focal plane of the objective is placed midway between the axis of rotation and the front face of the sample such that only one half of the sample is in focus at any given projection angle (as shown with the dashed line in Fig.1 c). The telecentricity of the lens allows us to use the highly efficient FBP reconstruction approach. LEDs emitting over a broad spectral range were chosen for their brightness and long life, and a custom circuit board was designed to minimize output flicker. The LED output was homogenized and collimated with off-the-shelf optics to ensure uniform illumination across the field of view. The stage, the camera, and the LEDs were controlled with a RaspberryPi^{TM} that interfaces with a central computer. A detailed description of the OptiJ hardware assembly, parts list, and system characterization can be found in the Supplementary Information.

OptiJ analysis. The reconstruction of a high-quality 3D volume from the OPT projections requires data pre-processing to avoid artifacts during reconstruction via FBP. OptiJ includes a set of freely available ImageJ/Fiji plugins to pre-process OPT data, as well as an efficient GPU-enabled FBP algorithm for reconstruction. The plugins and the suggested workflow for their use is shown in Fig. 2a. The Beer-Lambert correction plugin divides each tOPT projection by an average brightfield image following the Beer-Lambert Law(55) to obtain linear attenuation coefficients corrected for non-uniform pixel intensities, as demonstrated in the lower panel of Fig. 2b.i. A common artifact in OPT arises from the axis of rotation of the sample not being parallel to the plane of the FOV during acquisitions, which leads to the appearance of a shadow artifact around sharp features as demonstrated in Fig. 2b.ii. The Estimate Tilt and Offset plugin tracks a fiducial marker (such as a 100 µm glass bead) in the projections to determine if the axis of rotation is parallel to the center of the FOV, and produces correction values for the projection stack if this condition is not satisfied. These values can be used at the reconstruction step to minimize any shadow artifacts, as demonstrated in the corrected image in Fig. 2.b.ii. The Create Sinogram plugin displays a Radon Transform of the projections and uses the correction values for tilt and offset produced by the previous plugin to account for residual deviations, relaxing the need for thoroughly precise alignment of the system prior to acquisitions. The output of this plugin is a sinogram, an intermediate step in the FBP reconstruction named after its sinusoidal shape. Small sample wobble caused by mechanical jitter from low-cost stepper motors can be detected as jagged edges in an otherwise smooth sinogram, demonstrated in Fig. 2b.iii. The Dynamic Offset Correction plugin calculates a sinusoidal fit of the motion of a fiducial marker and uses the difference between the ideal fit coordinates and the actual motion of the bead to produce a jitter-free sinogram as shown in the corrected image in Fig. 2b.iii. This step concludes the pre-processing required to minimize artifacts prior to reconstruction. The 2D reconstruction plugin implements an FBP algorithm to reconstruct a 3D cross-sectional stack of the original object using the corrected sinogram. To speed up reconstruction

times via FBP, the plugin allows for GPU-enabled acceleration using OpenCL (56), which is open-source and platform-independent. This plugin also allows the user to choose from a variety of filters (Ramp, Hamming, Shepp-Logan, or no filter) for back-projection (15). A detailed description of the OptiJ plugin library, its functions and methods, usage and sample data for testing can be found in our online repository at https://lag-opt.github.io.

OPT of large organ samples. The non-destructive 3D imaging of whole lung lobes is very useful in the study of COPD models in mice, as it allows the identification of characteristic phenotypes such as bronchoconstriction (narrowing of airways), and the investigation of the extent of the structures affected in different lung areas. The superior, medial, and accessory lobes of the right lung, and the entire left lung of two adult mice were fixed, immunostained, cleared, and imaged using the OptiJ framework (see Supplementary Information for details on mice work). 512 raw projections were acquired over a full rotation of each lobe to obtain high-fidelity reconstructions. Two different proteins expressed in lung epithelial type 2 cells were targeted for fluorescent staining to determine which one allowed for better visualization of the structures critical to studying COPD, such as the bronchioles and alveolar sacs. The lobes of the first mouse were immunostained with a primary antibody against the Surfactant protein C, and the lobes from the second mouse with a primary antibody against the thyroid transcription factor type 1 (TTF-1). In both cases, a secondary antibody conjugated with an Alexa Fluor 488 dye was used to visualize the airway tree through eOPT. The labelling strategy targeting the Surfactant protein C revealed only gross features in the lobes' eOPT reconstructions, as demonstrated in the orthogonal views of the reconstructed stack from a large left lobe in Fig. 3a-d. The primary bronchus and some secondary and tertiary airways are indicated by red arrows in Fig. 3a-b, and the region in which the indiscernible finer features would be located, the parenchyma (lobe edge), is indicated by red arrowheads. The fluorescent signal collected with this labelling strategy is likely a combination of tissue autofluorescence originating mostly from collagen and the specific fluorescent signal from the dye. The alternative labelling strategy targeting the TTF-1 protein produced reconstructions with an improved signal-to-noise ratio and allowed the visualization of both large airways and minute bronchioles through the center and periphery of the lobes. The orthogonal views of the reconstructed stack from a medial lobe show both the primary and secondary bronchi (red arrows in Fig. 3e-f) and the higher order airways and tiny air sacs in the parenchyma (red arrowheads in Fig. 3.e-f). Figure 3h shows a 3D rendering of the entire medial lobe with a cut-out to direct attention to the intricate network of higher order airways that can be visualized inside the volume. We used Fourier Ring Correlation (FRC) (57) to estimate the resolution of the reconstructed stacks by splitting the data set into two stacks of 256 projections, and obtained a value of 50 µm (see Supplementary Information for details). The reconstructed lung lobes described in Fig. 3 can be viewed and explored interactively using the open-source data visualization platform FPBioimage (53). Volumetric models are available for immersive and interactive viewing directly in standard web browsers at our online repository, along with pre-recorded videos highlighting salient features in the reconstructions: https://lag-opt.github.io.

Discussion

OptiJ represents a low-cost open-source hardware and software implementation of OPT for the investigation of large volumetric samples. We demonstrate the imaging of whole organs in 3D with OptiJ at near-cellular resolution. The method reveals the structure of adult murine lungs, from the large primary bronchi to the minute bronchioles at the lung periphery. We compile and provide a novel open-source toolbox of image corrections for OPT measurements and detailed instructions for building a low-cost OPT setup. We present and address the hardware challenges introduced by low-cost OPT solutions. In particular, the sensitivity to sample alignment can be corrected by tracking a marker glass bead and compensating for the tilt using the OptiJ plugins provided. Additionally, we developed a novel Dynamic Offset Correction method to correct for jitter introduced by low-cost stepper motors used for sample rotation. These measures ensure both accuracy and repeatability in the recording of high-fidelity OPT data. Furthermore, we implemented for the first time Fourier Ring Correlation (FRC) as a resolution measure for reconstructed OPT data sets. The non-destructive 3D imaging of COPD mice models lung lobes could provide a whole-organ perspective of alveolar cell clusters in an intact lung, where the involvement of specific cell types in pathophysiological processes could be tracked and quantified, complementary to recent studies of COPD pathophysiology with confocal microscopy (58). Although immunostaining with the anti-surfactant protein C was only partially successful, we were able to make use of autofluorescence from elastin and collagen in epithelial cells and extracellular matrix from the large airway wall to boost signals and obtain high-contrast images of the large airway tree. More generally, the 3D imaging data of intact mouse organs enabled with OptiJ could be useful in tracking specific cell types, visualizing the heterogeneous distribution of disease, or assessing the effects of therapeutics in animal models of COPD. Newer tissue-clearing methods such as 3DISCO (59) and CLARITY (60) can also be implemented to improve on our current approach based on BaBB, which is known to introduce loss of fluorescent signal from certain dyes (61) and may cause linear shrinking of tissue (62). In summary, we provide a unique and complete set of calibration and reconstruction routines in a single ImageJ/Fiji plugin library along with a low-cost, easy to build and easy to use hardware set up. A previous implementation of the Radon transform exists in ImageJ/Fiji, but does not include calibration nor accelerated reconstruction algorithms (63). OptiJ implements both CPU and GPU acceleration for reconstructions, which yields reconstructions in tens of minutes rather than multiple hours. Furthermore, we demonstrate larger fields of view (13x8x8 mm^3) than most other OPT implementations (17, 22, 24, 28, 38), which typ-

ically range from 1x1x1 mm^3 to 5x5x5 mm^3. The larger field of view of OptiJ will be useful for examining anatomical structures and fluorescent signals from large model organisms (e.g. mouse, zebrafish, drosophila), organ samples from small animals or even organoids grown from pluripotent stem cells. Future work on OptiJ would include automation of the tilt and offset calibration routines with a direct feedback loop to the hardware after correction with the OptiJ plugins or implementation of deconvolution in OPT data using the model proposed by van der Horst (49). The research presented here was initially conducted in a collaborative effort by a cohort of 14 graduate students and formed part of their PhD training programme in the EPSRC Centre for Doctoral Training in Sensor Technologies and Applications. Students were given a minimal project brief and budget from which they developed a detailed technical proposal and work program. Individuals worked on subsections of the project (e.g. hardware prototyping, software development, biological sample preparation, and data gathering and analysis) with regular supervisory meetings to monitor progress and to identify bottlenecks. The project lasted over a period of 12 weeks and led to the development of a fully functioning prototype of the OPT device presented here. The overall goal was to develop high-end technology that is easily democratised through use of open technologies and open source software and that incentivises further deployment and development by the wider research community.

Materials and Methods

Animal ethics. Lung samples were obtained from two naïve C57/Black6 female mice which were humanely euthanised at the end of an independent experiment according to the European ethical guidelines of animal experimentation. The study was approved by the local Ethical committee in Gothenburg (EA137-2014).

Animal perfusion and tissue preparation. For the immunostaining of the lungs, mice were perfused through the right ventricle with PBS to remove blood from the tissue. Lungs were subsequently inflated with 4% PFA and fixed overnight at room temperature in fixative. Over the next 3 days, the lungs were rinsed in PBS and permeabilised through two cycles of dehydration-rehydration in a gradient of methanol, and in a solution of PBS and detergent (1% Triton X-100) to ensure antigens from the deepest part of the tissue were rendered accessible. All immunostains were then performed in 1% Triton X-100 in PBS (PBST) containing 10% of donkey serum. Two different immunostains were tested in separate lung samples with primary: i) anti-surfactant C protein antibody to target membrane antigen secreted from airway type 2 epithelial cells in alveoli or ii) anti-thyroid transcription factor-1 (TTF-1) antibody (Dako Agilent Products, mouse monoclonal, clone 8G7G3/1, Cat# M3575) to target nuclear antigen also present in airway type 2 epithelial cells. The lungs were incubated in primary antibody solution for 1h at room temperature and for 48h at 4°C followed by extensive washes with PBST and 1% foetal calf serum. Fluorescent labelling of the primary antibody was achieved with anti-IgG Alexa Fluor-488 secondary antibody in 1:500 dilution for 48h at 4°C followed by extensive washes for 3 hr to overnight. A detailed immunostaining protocol is available in the Supplementary Information.

Sample preparation. Fixed and immunostained samples were embedded in a 2% low-melting-point agarose (Thermofisher Part#R0801) solution as a holding medium for clearing and acquisition. 10 mL syringes were cut using a razor blade at the 1 mL and 6 mL mark. The syringe plunger was inserted from the 6 mL end just so the rubber tip was completely inside the cropped syringe tube. A pipette was used to fill approximately three quarters of the available volume in the tube with molten agarose. The agarose was left to cool for 3-10 minutes, and then samples were carefully transferred into the agarose-filled tube using smooth tweezers and were oriented close to the center of the tube. A spherical glass bead (Sigma-Aldrich Part#Z250465-1PAK) between 0.5 to 1 mm in diameter was immediately inserted close to the sample, but not in the same horizontal plane, as a tracking fiducial for alignment and calibration during post-processing. The exposed end of the tube was sealed with parafilm to avoid dehydration of the agarose during storage. Samples were placed in a fridge at 4°C for one hour to allow the solution to fully cross-link into solid agarose cylinders. The embedded lung lobes were pushed out of the syringes, dehydrated using 50% methanol for 24 hours and then 100% methanol for 48 hours, and then cleared using a 1:2 mixture of Benzyl alcohol and Benzyl benzoate (BaBB) for 72 hours, changing the BaBB solution every 24 hours. Prior to OPT acquisition, the agarose-embedded tissue cylinders were glued onto bright-zinc plated (BZP) penny washers (M5x25, Fixmart Part#402203217) using quick-dry epoxy (Loctite Epoxy Quick Set 0.85-Fluid Ounce Syringe, Henkel Corporation, Part#1395391). After the glue was cured, the penny washer was coupled to a magnetic kinematic mount (Thorlabs Part#SB1), ready to be inserted into the system for imaging. A detailed description of the preparation and mounting of the murine lung lobes can be found in the Supplementary Information.

Experimental setup. A 3D-printed flexure stage for open-source microscopy (54), was chosen for x,y,z translation and rotation of the sample because of its low cost (cost of printing material only) and modular design. An Andor CLARA camera with 6.45x6.45 μm^2 pixels was used for acquisition of the volume projections, although lower cost cameras can also be used. A 0.5x telecentric objective (Edmund Optics Part #63-741) with a 65 mm working distance and 0.028 NA was chosen to acquire the maximum field of view possible with the chosen detector. Two white light LEDs (Thorlabs Part #MWWHD3) were chosen to provide even illumination with minimal flicker. These were fitted in small cage systems with an optical diffuser (Thorlabs Part#DG10-600), an adjustable iris (Thorlabs Part #SM1D12D), and a condenser lens (Thorlabs Part #LA1401-A). A GFP excitation and emission filter pair was used for eOPT (Excitation: 482/25 Part#FF01-

482/25-25, Emission: 515/LP Part#FF01-515/LP-25, Semrock). A Hellma glass cuvette (Z805750-1EA, Scientific Laboratory Supplies) was used as the immersion chamber for the sample during imaging. The filled chamber was raised using a Swiss Boy lab jack (Sigma Aldrich Part#2635316-1EA) to completely cover the agarose gel containing the sample during the acquisitions with the BaBB. The acquisition software was written in Java and packaged as an independent executable file. eOPT and tOPT projections were acquired with exposure times of 300 ms and 1 ms, respectively. Pictures of the set-up, a list of parts, instructions for assembly, information about the acquisition software, and the characterization of the x, y, and z motion of the stage can be found in the Supplementary Information.

Software for image reconstruction. The reconstruction and calibration routines in OptiJ were written in Java and integrated as a plugin library in ImageJ (51), a standard open-source platform for image analysis. OptiJ is available for download online, along with an instruction manual, source code, and examples of use at: https://lag-opt.github.io. The interactive web application FPBioimage was used to visualize the three-dimensional reconstructions of the OPT data used in Fig.3. The reconstructed data sets can be used to visualized and explored online using FPBioimage as well, following the instructions in our online repository.

Data availability statement. All the raw and processed data, instruction manuals, and code used for this study can be found in our online repository at https://lag-opt.github.io.

ACKNOWLEDGEMENTS

A functional OPT system prototype was prepared and delivered by the 2015-2016 Sensor Centre for Doctoral Training (CDT) cohort from the University of Cambridge. We thank AstraZeneca PLC for providing dehydrated and stained murine lung samples for imaging and James McGinty and Thomas Watson for fruitful conversations on OPT. We also thank Ricardo Henriques for his neatly formatted BioRxiv preprint LateX template. This work is supported by grants from the UK Engineering and Physical Sciences Research Council, the EPSRC (grants EP/L015889/1 and EP/H018301/1), the Gates Cambridge Scholarship (PVR), the federal government of Nigeria through the Presidential Special Scholarship for Innovation and Development managed by NUC and funded by PTDF (PO), the Wellcome Trust (grants 203249/Z/16/Z and 089703/Z/09/Z), the UK Medical Research Council (MRC) (grants MR/K015850/1 and MR/K02292X/1), MedImmune, the RCUK under the Technology Touching Life Initiative, and Infinitus China Ltd. RFL also acknowledges the support of the UK Biotechnology and Biological Sciences Research Council (BBSRC) TRDF grants (BB/P027431/1 and BB/R021805/1). FS also acknowledges the support from European Molecular Biology Organisation (#7411) and Marie Skłodowska-Curie Actions (#836355).

AUTHOR CONTRIBUTIONS

P.V.R. did imaging experiments with the mouse lungs, wrote the manuscript, and characterized the OPT system. J.Z. wrote and compiled the suite of calibration and reconstruction routines for the OptiJ software. F-X.B, R.F.L, O.V., F.S., E.J.R., and C.F.K reviewed the manuscript and provided useful feedback. P.V.R. and F-X.B. cleared and mounted the murine lungs. O.V. conducted experiments to test early versions of the OptiJ hardware and software components. X-H.Z. perfused and immunostained the murine lungs. F.R. designed and machined the translation and rotation stage for the OptiJ hardware, and designed and built the custom circuit boards used to power and control the LEDs and the stage motors. B.F.S. coordinated the software development, proposed the software tilt and background correction methods, developed the camera interface, and designed the graphical user interface (GUI). P.O. designed, implemented, tested, and packaged the graphical user interface (GUI), and image acquisition software. G.G. made the CAD drawings and wrote assembly instructions for the OptiJ hardware. S.S. tested GPU acceleration in filtered back-projection with preliminary MATLAB scripts. C.V. was the project leader for the Sensor CDT 2015 cohort. O.S. designed the OPT sample holder for 1 mL syringes. F.A. devised the syringe mounting strategy for OPT samples. A.S. prepared early test samples of mice gonads. D.S. characterised the opto-mechanic properties of the OPT, including optical resolution, camera sensitivity and stage positioning errors. F.S. and R.F.L. provided useful advice and helped write software for the OptiJ calibration routines. R.F.L. wrote calibration software in MATLAB to quantify the misalignment of the samples. O.H., R.F.L. and F.S. provided guidance and mentoring for the Sensor CDT 2015-2016 cohort. C.F.K, R.F.L. and F.S. devised the project and organized the Sensor CDT 2015-2016 cohort.

COMPETING FINANCIAL INTERESTS

The authors declare no competing financial interests.

Bibliography

1. Jon O. Cleary, Anthony N. Price, David L. Thomas, Peter J. Scambler, Vanessa Kyriakopoulou, Karen McCue, Jürgen E. Schneider, Roger J. Ordidge, and Mark F. Lythgoe. Cardiac phenotyping in ex vivo murine embryos using μMRI. *NMR in Biomedicine*, 22(8): 857–866, 2009. ISSN 09523480. doi: 10.1002/nbm.1400.
2. Bruce Fischl, Allison A. Stevens, Niranjini Rajendran, B. T Thomas Yeo, Douglas N. Greve, Koen Van Leemput, Jonathan R. Polimeni, Sita Kakunoori, Randy L. Buckner, Jennifer Pacheco, David H. Salat, Jennifer Melcher, Matthew P. Frosch, Bradley T. Hyman, P. Ellen Grant, Bruce R. Rosen, André J W van der Kouwe, Graham C. Wiggins, Lawrence L. Wald, and Jean C. Augustinack. Predicting the location of entorhinal cortex from MRI. *NeuroImage*, 47(1):8–17, 2009. ISSN 10538119. doi: 10.1016/j.neuroimage.2009.04.033.
3. Cesar A. Berrios-Otero, Youssef Zaim Wadghiri, Brian J. Nieman, Alexandra L. Joyner, and Daniel H. Turnbull. Three-dimensional micro-MRI analysis of cerebral artery development in mouse embryos. *Magnetic Resonance in Medicine*, 62(6):1431–1439, 2009. ISSN 07403194. doi: 10.1002/mrm.22113.
4. Christof Baltes, Nicole Radzwill, Simone Bosshard, Daniel Marek, and Markus Rudin. Micro MRI of the mouse brain using a novel 400 MHz cryogenic quadrature RF probe. *NMR in Biomedicine*, 22(8):834–842, 2009. ISSN 09523480. doi: 10.1002/nbm.1396.
5. P. Ruegsegger, B. Koller, and R. Muller. A microtomographic system for the nondestructive evaluation of bone architecture. *Calcified Tissue International*, 58(1):24–29, 1996. ISSN 0171967X. doi: 10.1007/s002239900006.
6. Alex de Crespigny, Hani Bou-Reslan, Merry C. Nishimura, Heidi Phillips, R. A D Carano, and Helen E. D'Arceuil. 3D micro-CT imaging of the postmortem brain. *Journal of Neuroscience Methods*, 171(2):207–213, 2008. ISSN 01650270. doi: 10.1016/j.jneumeth.2008.03.006.
7. J. C. Hogg, J. E. McDonough, P. G. Sanchez, J. D. Cooper, H. O. Coxson, W. M. Elliott, D. Naiman, M. Pochettino, D. Horng, W. B. Gefter, and A. C. Wright. Micro-Computed Tomography Measurements of Peripheral Lung Pathology in Chronic Obstructive Pulmonary Disease. *Proceedings of the American Thoracic Society*, 6(6):546–549, 2009. ISSN 1546-3222. doi: 10.1513/pats.200905-029DS.
8. John E McDonough, Ren Yuan, Masaru Suzuki, Nazgol Seyednejad, W Mark Elliott, Pablo G Sanchez, Alexander C Wright, Warren B Gefter, Leslie Litzky, Harvey O Coxson, Peter D Paré, Don D Sin, Richard A Pierce, Jason C Woods, Annette M McWilliams, John R Mayo, Stephen C Lam, Joel D Cooper, and James C Hogg. Small-Airway Obstruction and Emphysema in Chronic Obstructive Pulmonary Disease. *New England Journal of Medicine*, 365(17):1567–1575, 2011. doi: 10.1056/NEJMoa1301150.
9. M. D. Wong, A. E. Dorr, J. R. Walls, J. P. Lerch, and R. M. Henkelman. A novel 3D mouse embryo atlas based on micro-CT. *Development*, 139(17):3248–3256, 2012. ISSN 0950-1991. doi: 10.1242/dev.082016.
10. C. J.R. Sheppard and A. Choudhury. Image formation in the scanning microscope. *Optica Acta*, 24(10):1051–1073, 1977. ISSN 00303909. doi: 10.1080/713819421.
11. Jan Huisken, Jim Swoger, Filippo Del Bene, Joachim Wittbrodt, and Ernst H K Stelzer. Live Embryos by Selective Plane Illumination Microscopy. *Science*, 305(August):1007–1010, 2004.
12. Philipp J. Keller and Ernst HK Stelzer. Quantitative in vivo imaging of entire embryos with Digital Scanned Laser Light Sheet Fluorescence Microscopy, 2008. ISSN 09594388.
13. Hans Ulrich Dodt, Ulrich Leischner, Anja Schierloh, Nina Jährling, Christoph Peter Mauch, Katrin Deininger, Jan Michael Deussing, Matthias Eder, Walter Zieglgänsberger, and Klaus Becker. Ultramicroscopy: Three-dimensional visualization of neuronal networks in the whole mouse brain. *Nature Methods*, 4(4):331–336, 2007. ISSN 15487091. doi: 10.1038/nmeth1036.
14. J. Sharpe. Optical Projection Tomography as a Tool for 3D Microscopy and Gene Expression Studies. *Science*, 296(5567):541–545, 2002. ISSN 00368075. doi: 10.1126/science.1068206.
15. A.C. Kak and Malcolm Slaney. *Principles of Computerized Tomography*. IEEE Press, 1988.
16. Janet Kerwin, Mark Scott, James Sharpe, Luis Puelles, Stephen C Robson, Margaret Martínez-de-la Torre, Jose Luis Ferran, Guangjie Feng, Richard Baldock, Tom Strachan, Duncan Davidson, and Susan Lindsay. 3 Dimensional Modelling of Early Human Brain Development Using Optical Projection Tomography. *BMC neuroscience*, 5:27, 2004. ISSN 1471-2202. doi: 10.1186/1471-2202-5-27.
17. Johnathon R. Walls, Leigh Coultas, Janet Rossant, and R. Mark Henkelman. Three-dimensional analysis of vascular development in the mouse embryo. *PLoS ONE*, 3(8), 2008. ISSN 19326203. doi: 10.1371/journal.pone.0002853.
18. Jacqueline a. Gleave, Michael D. Wong, Jun Dazai, Maliha Altaf, R. Mark Henkelman, Jason P. Lerch, and Brian J. Nieman. Neuroanatomical phenotyping of the mouse brain with three-dimensional autofluorescence imaging. *Physiological Genomics*, 44(June 2012):778–785, 2012. ISSN 1531-2267. doi: 10.1152/physiolgenomics.00055.2012.
19. Manuela Kellner, Marko Heidrich, Rebecca Beigel, Raoul-Amadeus Lorbeer, Lars Knudsen, Tammo Ripken, Alexander Heisterkamp, Heiko Meyer, Mark Philipp Kühnel, and Matthias Ochs. Imaging of the mouse lung with scanning laser optical tomography (SLOT). *Journal of applied physiology (Bethesda, Md. : 1985)*, 113(6):975–83, 2012. ISSN 1522-1601. doi: 10.1152/japplphysiol.00026.2012.
20. Gregory a Anderson, Michael D Wong, Jian Yang, and R Mark Henkelman. 3D imaging, registration, and analysis of the early mouse embryonic vasculature. *Developmental dynamics : an official publication of the American Association of Anatomists*, 242(5):527–38, 2013. ISSN 1097-0177. doi: 10.1002/dvdy.23947.

21. Emilio J Gualda, Tiago Vale, Pedro Almada, José A Feijó, Gabriel G Martins, and Nuno Moreno. OpenSpinMicroscopy: an open-source integrated microscopy platform. *Nature Methods*, 10(7):599–600, 2013. ISSN 1548-7091. doi: 10.1038/nmeth.2508.
22. Jürgen Mayer, Alexandre Robert-Moreno, Renzo Danuser, Jens V. Stein, James Sharpe, and Jim Swoger. OPTiSPIM: integrating optical projection tomography in light sheet microscopy extends specimen characterization to nonfluorescent contrasts. *Optics letters*, 39 (4), 2014. ISSN 1539-4794. doi: 10.1364/OL.39.001053.
23. Manmohan Singh, Raksha Raghunathan, Victor Piazza, Anjul M. Davis-Loiacono, Alex Cable, Tegy J. Vedakkan, Trevor Janecek, Michael V. Frazier, Achuth Nair, Chen Wu, Irina V. Larina, Mary E. Dickinson, and Kirill V. Larin. Applicability, usability, and limitations of murine embryonic imaging with optical coherence tomography and optical projection tomography. *Biomedical Optics Express*, 7(6):2295, 2016. ISSN 2156-7085. doi: 10.1364/BOE.7.002295.
24. Thomas Watson, Natalie Andrews, Samuel Davis, Laurence Bugeon, D Dallman, and James Mcginty. OPTiM : Optical projection tomography integrated microscope using open-source hardware and software. *PLoS ONE*, pages 1–13, 2017.
25. D Avid N Guyen, P A U L J M Archand, A L Rielle, P Lanchette, J Ulia N Ilsson, M Iguel S Ison, J Érôme, E Xtermann, A Ntonio L Opez, M Arcin S Ylwestrzak, J Essica S Ordet Essimoz, A N J A S Chmidt Hristensen, D An, H Olmberg, D Imitri V A N D E V Ille, and T H E O L Asser. Optical projection tomography for rapid whole mouse brain imaging. *Biomedical Optics Express*, 8(12):331–336, 2017.
26. Tomas Alanentalo, Amir Asayesh, Harris Morrison, Christina E. Lorén, Dan Holmberg, James Sharpe, and Ulf Ahlgren. Tomographic molecular imaging and 3D quantification within adult mouse organs. *Nature Methods*, 4(1):31–33, 2007. ISSN 15487091. doi: 10.1038/nmeth985.
27. Andreas Hörnblad, Abbas Cheddad, and Ulf Ahlgren. An improved protocol for optical projection tomography imaging reveals lobular heterogeneities in pancreatic islet and β-cell mass distribution. *Islets*, 3(4):204–208, 2011. ISSN 19382014. doi: 10.4161/isl.3.4.16417.
28. James McGinty, Khadija B. Tahir, Romain Laine, Clifford B. Talbot, Christopher Dunsby, Mark A A Neil, Laura Quintana, James Swoger, James Sharpe, and Paul M W French. Fluorescence lifetime optical projection tomography. *Journal of Biophotonics*, 1(5):390–394, 2008. ISSN 1864063X. doi: 10.1002/jbio.200810044.
29. Andrea Bassi, Luca Fieramonti, Cosimo D'Andrea, Marina Mione, Gianluca Valentini, and Cosimo D'Andrea. In vivo label-free three-dimensional imaging of zebrafish vasculature with optical projection tomography. *Journal of biomedical optics*, 16(10):100502, 2011. ISSN 1560-2281. doi: 10.1117/1.3640808.
30. Luca Fieramonti, Andrea Bassi, Efrem Alessandro Foglia, Anna Pistocchi, Cosimo D'Andrea, Gianluca Valentini, Rinaldo Cubeddu, Sandro de Silvestri, Giulio Cerullo, and Franco Cotelli. Time-Gated Optical Projection Tomography Allows Visualization of Adult Zebrafish Internal Structures. *PLoS ONE*, 7(11):1–7, 2012. ISSN 19326203. doi: 10.1371/journal.pone.0050744.
31. Teresa Correia, Nicola Lockwood, Sunil Kumar, Jun Yin, Marie Christine Ramel, Natalie Andrews, Matilda Katan, Laurence Bugeon, Margaret J. Dallman, James McGinty, Paul Frankel, Paul M W French, and Simon Arridge. Accelerated optical projection tomography applied to in vivo imaging of zebrafish. *PLoS ONE*, 10(8):1–17, 2015. ISSN 19326203. doi: 10.1371/journal.pone.0136213.
32. Natalie Andrews, Marie Christine Ramel, Sunil Kumar, Yuriy Alexandrov, Douglas J. Kelly, Sean C. Warren, Louise Kerry, Nicola Lockwood, Antonina Frolov, Paul Frankel, Laurence Bugeon, James Mcginty, Margaret J. Dallman, and Paul M W French. Visualising apoptosis in live zebrafish using fluorescence lifetime imaging with optical projection tomography to map FRET biosensor activity in space and time. *Journal of Biophotonics*, 9(4):414–424, 2016. ISSN 18640648. doi: 10.1002/jbio.201500258.
33. Sunil Kumar, Nicola Lockwood, Marie-Christine Ramel, Teresa Correia, Matthew Ellis, Yuriy Alexandrov, Natalie Andrews, Rachel Patel, Laurence Bugeon, Margaret J. Dallman, Sebastian Brandner, Simon Arridge, Matilda Katan, James McGinty, Paul Frankel, and Paul M. W. French. Quantitative in vivo optical tomography of cancer progression & vasculature development in adult zebrafish. *Oncotarget*, 5(28):2–11, 2016. ISSN 1949-2553. doi: 10.18632/oncotarget.9756.
34. A. Bassi, B. Schmid, and J. Huisken. Optical tomography complements light sheet microscopy for in toto imaging of zebrafish development. *Development*, 142(5):1016–1020, 2015. ISSN 0950-1991. doi: 10.1242/dev.116970.
35. Leeanne McGurk, Harris Morrison, Liam P. Keegan, James Sharpe, and Mary A. O'Connell. Three-dimensional imaging of Drosophila melanogaster. *PLoS ONE*, 2(9), 2007. ISSN 19326203. doi: 10.1371/journal.pone.0000834.
36. Heiko Meyer, Alex Darrell, Athanasios Metaxakis, Charalambos Savakis, and Jorge Ripoll. Optical Projection Tomography for In-Vivo Imaging of Drosophila melanogaster. *Microscopy and Analysis*, 22(5):19–21, 2008.
37. Claudio Vinegoni, Chrysoula Pitsouli, Daniel Razansky, Norbert Perrimon, and Vasilis Ntziachristos. In vivo imaging of Drosophila melanogaster pupae with mesoscopic fluorescence tomography. *Nature Methods*, 5(1):45–47, 2008. ISSN 15487091. doi: 10.1038/nmeth1149.
38. Alicia Arranz, Di Dong, Shouping Zhu, Charalambos Savakis, Jie Tian, and Jorge Ripoll. In-vivo optical tomography of small scattering specimens: Time-lapse 3D imaging of the head eversion process in Drosophila melanogaster. *Scientific Reports*, 4:1–5, 2014. ISSN 20452322. doi: 10.1038/srep07325.
39. K. Lee, Jerome Avondo, Harris Morrison, Lilian Blot, Margaret Stark, James Sharpe, Andrew Bangham, and Enrico Coen. Visualizing Plant Development and Gene Expression in Three Dimensions Using Optical Projection Tomography. *the Plant Cell*, 18(9):2145–2156, 2006. ISSN 1040-4651. doi: 10.1105/tpc.106.043042.
40. Karen J.I. Lee, Grant M. Calder, Christopher R. Hindle, Jacob L. Newman, Simon N. Robinson, Jerome J.H.Y. Avondo, and Enrico S. Coen. Macro optical projection tomography for large scale 3D imaging of plant structures and gene activity. *Journal of Experimental Botany*, 68(3):527–538, 2017. ISSN 14602431. doi: 10.1093/jxb/erw452.
41. Matthias Rieckher, Udo Jochen Birk, Heiko Meyer, Jorge Ripoll, and Nektarios Tavernarakis. Microscopic optical projection tomography in vivo. *PLoS ONE*, 6(4):2–7, 2011. ISSN 19326203. doi: 10.1371/journal.pone.0018963.
42. Varsha Kumar, Elke Scandella, Renzo Danuser, Lucas Onder, Maximilian Nitschké, Yoshinori Fukui, Cornelia Halin, Burkhard Ludewig, and Jens V. Stein. Global lymphoid tissue remodeling during a viral infection is orchestrated by a B cell-lymphotoxin-dependent pathway. *Blood*, 115(23):4725–4733, 2010. ISSN 00064971. doi: 10.1182/blood-2009-10-250118.
43. Alicia Arranz, Di Dong, Shouping Zhu, Markus Rudin, Christos Tsatsanis, Jie Tian, and Jorge Ripoll. Helical optical projection tomography. *Optics Express*, 21(22):25912, 2013. ISSN 1094-4087. doi: 10.1364/OE.21.025912.
44. Tomas Alanentalo, Andreas Hörnblad, Sofia Mayans, Anna Karin Nilsson, James Sharpe, Asa Larefalk, Ulf Ahlgren, and Dan Holmberg. Quantification and three-dimensional imaging of the insulitis-induced destruction of beta-cells in murine type 1 diabetes. *Diabetes*, 59(7):1756–1764, 2010. ISSN 1939-327X. doi: 10.2337/db09-1400.U.A.
45. Malcolm E. Fisher, Allyson K. Clelland, Andrew Bain, Richard A. Baldock, Paula Murphy, Helen Downie, Cheryll Tickle, Duncan R. Davidson, and Richard A. Buckland. Integrating technologies for comparing 3D gene expression domains in the developing chick limb. *Developmental Biology*, 317(1):13–23, 2008. ISSN 00121606. doi: 10.1016/j.ydbio.2008.01.031.
46. Jean-François Colas and James Sharpe. Live optical projection tomography. *Organogenesis*, 5(4):211–6, 2009. ISSN 1555-8592. doi: 10.1007/978-3-540-68993-5_9.
47. Edite Figueiras, Ana M Soto, Danilo Jesus, M Lehti, J Koivisto, J E Parraga, J Silva-Correia, J M Oliveira, R L Reis, M Kellomäki, and J Hyttinen. Optical projection tomography as a tool for 3D imaging of hydrogels. *Biomedical optics express*, 5(10):3443–3449, 2014. ISSN 2156-7085. doi: 10.1364/BOE.5.003443.
48. Johnathon R. Walls, John G. Sled, James Sharpe, and R. Mark Henkelman. Correction of artefacts in optical projection tomography. *Physics in Medicine and Biology*, 50(19):4645–4665, 2005. ISSN 00319155. doi: 10.1088/0031-9155/50/19/015.
49. Jelle van der Horst and Jeroen Kalkman. Image resolution and deconvolution in optical tomography. *Opt. Express*, 24(21):24460–24472, 2016. ISSN 1094-4087. doi: 10.1364/OE.24.024460.
50. J McGinty, H B Taylor, L Chen, L Bugeon, J R Lamb, M J Dallman, and P M French. In vivo fluorescence lifetime optical projection tomography. *Biomed Opt Express*, 2(5):1340–1350, 2011. ISSN 1864063X. doi: 10.1364/BOE.2.001340.
51. Johannes Schindelin, Ignacio Arganda-Carreras, Erwin Frise, Verena Kaynig, Mark Longair, Tobias Pietzsch, Stephan Preibisch, Curtis Rueden, Stephan Saalfeld, Benjamin Schmid, Jean-Yves Tinevez, Daniel James White, Volker Hartenstein, Kevin Eliceiri, Pavel Tomancak, and Albert Cardona. Fiji: an open-source platform for biological-image analysis. *Nat Meth*, 9(7):676–682, jul 2012. ISSN 1548-7091.
52. Michael D. Wong, Jun Dazai, Johnathon R. Walls, Nicholas W. Gale, and R. Mark Henkelman. Design and Implementation of a Custom Built Optical Projection Tomography System. *PLoS ONE*, 8(9), 2013. ISSN 19326203. doi: 10.1371/journal.pone.0073491.
53. Marcus Fantham and Clemens F Kaminski. A new online tool for visualization of volumetric data. *Nature Photonics*, 11(2):69, 2017. ISSN 1749-4885. doi: 10.1038/nphoton.2016.273.
54. James P. Sharkey, Darryl C W Foo, Alexandre Kabla, Jeremy J. Baumberg, and Richard W. Bowman. A one-piece 3D printed flexure translation stage for open-source microscopy. *Review of Scientific Instruments*, 87(2), 2016. ISSN 10897623. doi: 10.1063/1.4941068.
55. D. F. Swinehart. The Beer-Lambert Law. *Journal of Chemical Education*, 39(7):333, 1962. ISSN 0021-9584. doi: 10.1021/ed039p333.
56. John E Stone, David Gohara, and Guochun Shi. OpenCL: A Parallel Programming Standard for Heterogeneous Computing Systems. *Computing in science & engineering*, 12(3):66–72, may 2010. ISSN 1521-9615. doi: 10.1109/MCSE.2010.69.
57. Robert P.J. Nieuwenhuizen, Keith A. Lidke, Mark Bates, Daniela Leyton Puig, David Grünwald, Sjoerd Stallinga, and Bernd Rieger. Measuring image resolution in optical nanoscopy. *Nature Methods*, 10(6):557–562, 2013. ISSN 15487091. doi: 10.1038/nmeth.2448.
58. Eline M Van Dijk, Sule Culha, Mark H Menzen, and Cécile M Bidan. Elastase-Induced Parenchymal Disruption and Airway Hyper Responsiveness in Mouse Precision Cut Lung Slices : Toward an Ex vivo COPD Model. *Frontiers in Physiology*, 7(January):1–11, 2017. doi: 10.3389/fphys.2016.00657.
59. Ali Ertürk, Klaus Becker, Nina Jährling, Christoph P. Mauch, Caroline D. Hojer, Jackson G. Egen, Farida Hellal, Frank Bradke, Morgan Sheng, and Hans Ulrich Dodt. Three-dimensional imaging of solvent-cleared organs using 3DISCO. *Nature Protocols*, 7(11):1983–1995, 2012. ISSN 17542189. doi: 10.1038/nprot.2012.119.
60. Kwanghun Chung, Jenelle Wallace, Sung Yon Kim, Sandhiya Kalyanasundaram, Aaron S. Andalman, Thomas J. Davidson, Julie J. Mirzabekov, Kelly A. Zalocusky, Joanna Mattis, Aleksandra K. Denisin, Sally Pak, Hannah Bernstein, Charu Ramakrishnan, Logan Grosenick, Viviana Gradinaru, and Karl Deisseroth. Structural and molecular interrogation of intact biological systems. *Nature*, 497(7449):332–337, 2013. ISSN 00280836. doi: 10.1038/nature12107.
61. T. Kuwajima, A. A. Sitko, P. Bhansali, C. Jurgens, W. Guido, and C. Mason. ClearT: a detergent- and solvent-free clearing method for neuronal and non-neuronal tissue. *Development*, 140(6):1364–1368, 2013. ISSN 0950-1991. doi: 10.1242/dev.091844.
62. Meng Tsen Ke, Satoshi Fujimoto, and Takeshi Imai. SeeDB: A simple and morphology-preserving optical clearing agent for neuronal circuit reconstruction. *Nature Neuroscience*, 16(8):1154–1161, 2013. ISSN 10976256. doi: 10.1038/nn.3447.
63. Damien Farrell. Radon Transform ImageJ plugin, 2016.